

Magneto-optical Study of Zeeman Effect in Mn modulation-doped InAs/InGaAs/InAlAs Quantum Well Structures

Ya. V. Terent'ev^{1,2}, S. N. Danilov¹, H. Plank¹, J. Loher¹, D. Schuh¹, D. Bougeard¹, D. Weiss¹, M. V. Durnev², S. A. Tarasenko^{2,3}, I. V. Rozhansky^{2,3}, S. V. Ivanov², D. R. Yakovlev^{2,4}, and S. D. Ganichev¹

¹ *Physics Department, University of Regensburg, 93040 Regensburg, Germany*

² *Ioffe Physical-Technical Institute, 194021 St. Petersburg, Russia*

³ *St. Petersburg State Polytechnic University, 195251 St. Petersburg, Russia and*

⁴ *Experimentelle Physik 2, Technische Universität Dortmund, 44227 Dortmund, Germany*

We report on a magneto-photoluminescence (PL) study of Mn modulation-doped InAs/InGaAs/InAlAs quantum wells. Two PL lines corresponding to the radiative recombination of photoelectrons with free and bound-on-Mn holes have been observed. In the presence of a magnetic field applied in the Faraday geometry both lines split into two circularly polarized components. While temperature and magnetic field dependences of the splitting are well described by the Brillouin function, providing an evidence for exchange interaction with spin polarized manganese ions, the value of the splitting exceeds the expected value of the giant Zeeman splitting by two orders of magnitude for a given Mn density. Possible reasons of this striking observation are discussed.

I. INTRODUCTION

Implementation of spintronics concepts requires semiconductor heterostructures with evident magnetic properties. To enhance the interaction between carrier spins and a magnetic field and to achieve ferromagnetic spin ordering heavy doping of materials with magnetic ions is required. Diluted magnetic semiconductors (DMS) based on narrow-gap III-V compounds, and in particular InMnAs, are considered to be promising candidates for application due to a relatively high Curie temperature and the strong spin-orbit interaction [1, 2]. While InAs-based DMS systems with strong spin-orbit coupling have been realized and show very interesting magnetotransport [3–5] and opto-electronic properties [6–10], direct measurements of the giant Zeeman splitting by means of polarized magneto-photoluminescence (PL) have not been reported so far. This is primary caused by the fact that the doping of III-V compounds by Mn atoms generates numerous lattice defects (even if they are partially removed by annealing [2]) and, consequently, to a drastic decrease of the radiation efficiency. This obstacle can be overcome in InAs quantum wells (QW) in which the barrier is modulation-doped with Mn and Mn atoms are transported by segregation into the InAs QW.

Here, we study the magneto-PL of high-quality DMS heterostructures InAs/In_{0.75}Ga_{0.25}As/In_{0.75}Al_{0.25}As:Mn, where small concentration of Mn in the InAs QW was provided by segregation. In zero magnetic field, the low-temperature PL is contributed by two lines separated by 25 meV. The analysis shows that the observed PL lines stem from the recombination of free and bound-on-Mn holes with photoexcited electrons. A magnetic field applied in the Faraday geometry results in the splitting of each PL line into two circularly polarized components with the opposite helicity. The splitting is found to be a

nonlinear function of the magnetic field and strong temperature dependent. These findings are qualitatively well described by the presented theory which takes into account radiative recombination processes in the InAs QW and the exchange interaction of carriers with spin polarized Mn ions. At the same time, the value of the splitting exceeds the expected giant Zeeman splitting by two orders of magnitude. Possible reasons of this striking observation are discussed.

II. SAMPLES

The InAs/In_{0.75}Ga_{0.25}As/In_{0.75}Al_{0.25}As QW heterostructures investigated were fabricated by molecular beam epitaxy (MBE) on a fully relaxed metamorphic In_xAl_{1-x}As/(001)GaAs compositionally graded buffer where the In content x is increased stepwise from 0.05 to 0.75 over 1 μm of layer thickness. Such an approach on structure design enables the fabrication of high quality defect-free and strain relaxed virtual substrates of high indium content that allow an effective collection of photogenerated carriers into the QW [11].

All experimental samples share the same QW design. Following the band lineups sketched on Fig. 1 an In_{0.75}Ga_{0.25}As shallow QW embedded in between In_{0.75}Al_{0.25}As barriers features an asymmetrically inserted and compressively strained InAs channel of 4 nm. The distances between the InAs channel edges and the left and right InAlAs/InGaAs interfaces are 2.5 nm and 13.5 nm, respectively. Manganese containing samples possess 7 nm layers of homogeneously Mn doped In_{0.75}Al_{0.25}As that are inserted on the substrate side of the QW region and separated from the QW by an In_{0.75}Al_{0.25}As barrier of 5 nm thickness. Due to a segregation effect during the MBE growth process a significant amount of manganese resides in the vicinity of the

InAs QW. Two structures, A and B, with different Mn concentration were realized. The sample, referred as A in this paper, has a dopant concentration not exceeding $n_{Mn} = 2 \times 10^{20} \text{ cm}^{-3}$ that results in a Mn concentration of about two orders of magnitude lower in the InAs QW as revealed by secondary ion mass spectrometry (SIMS) [12]. Having an acceptor nature in III-V compounds Mn provides a two-dimensional hole gas (2DHG) in the InAs:Mn QW. Hall effect measurements determined a hole density as high as 10^{12} cm^{-2} at $T = 4.2 \text{ K}$. As for the second structure B of the same design but of significantly lower doping concentration (653°C vs 852°C temperature of Mn effusion cell) conclusively a two times lower hole density was measured in magneto-transport experiments. In addition to these diluted magnetic semiconductors (DMS) QWs an intentionally undoped structure R without any Mn implementation was grown to serve as a reference.

III. EXPERIMENTAL TECHNIQUE

In our experiments we have used an experimental setup designed to measure polarization resolved magneto-PL in the infrared (IR) wavelength regime ($2 \div 5 \mu\text{m}$). The setup includes a magneto-optical helium bath cryostat, a laser diode excitation source, an optical polarization system and a grating or Fourier spectrometer equipped with a nitrogen cooled IR photodetector. Spectra are recorded by using lock-in technique. Magnetic fields up to 6 T were applied normally to the sample plain and along the wave vector of the emission, i.e., the experiment is done in Faraday geometry. The sample temperature can be varied from 2 up to 300 K. The laser diode, operating in *cw* mode, emits at wavelength $\lambda = 809 \text{ nm}$ and is focused onto a 1 mm diameter spot at the surface of the sample. The excitation density W_{exc} can be changed from 0.5 to

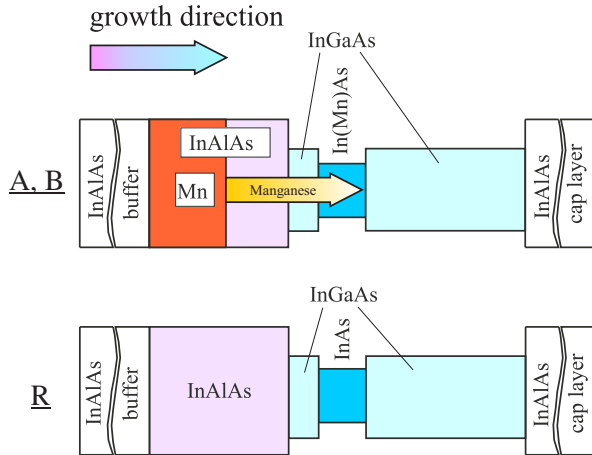


FIG. 1: Band diagrams of the QW structures under study excluding the substrate and the InAlAs graded buffer.

20 W/cm^2 . The PL emission passes through a polarization system consisting of a quarter wavelength retardation ZnSe Fresnel rhomb and a linear polarizer having the optical axes crossed at an angle of $\pm 45^\circ$ to select σ^+ or σ^- polarized light [13, 14].

IV. EXPERIMENTAL RESULTS

All samples studied showed bright PL although the signal from DMS samples was much weaker than that from the reference structure. The signal depends linearly on the excitation density in the explored range $W_{exc} = 0.5 \div 20 \text{ W/cm}^2$.

The PL band of sample A exhibits two contributions marked in Fig. 2(a) as Peak I and Peak II, which are separated from each other by about 25 meV. In a magnetic field, both Peak I and Peak II are blue shifted and split into two circularly polarized components, Fig. 2(b). Splitting reaches a large value up to 6 meV, Fig. 3. At low temperatures, the magnetic field dependence of the energy splitting of Peak I tends to saturate, see Fig. 4. Increasing the temperatures above 15 K, we observe that the splitting of both peaks rapidly vanishes, Fig. 4.

Peak I is σ^- polarized whereas the polarization of Peak II is opposite. The degree of circular polarization of Peak I, $P_{circ} = \frac{I_+ - I_-}{I_+ + I_-} \times 100\%$, where $I_{+/-}$ is the intensity of $\sigma^{+/-}$ polarized emission, reaches 30% at $B = 6 \text{ T}$.

Figure 5 shows the magnetic field dependence of the

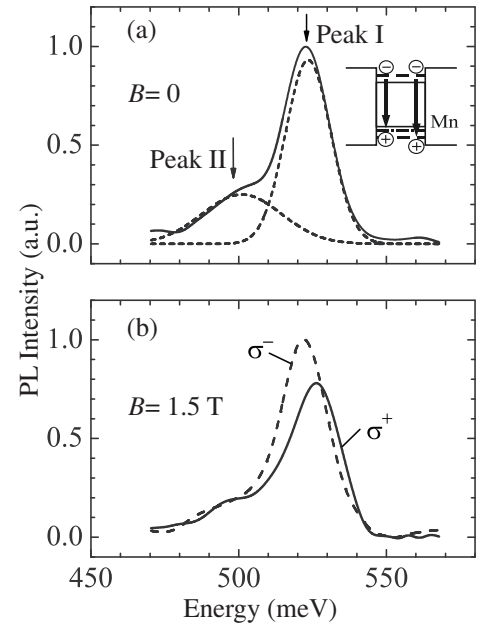


FIG. 2: PL spectra of sample A measured at $T = 2 \text{ K}$ and $W_{exc} = 10 \text{ W/cm}^2$. (a) No magnetic field is applied, (b) circularly polarized magneto-PL spectra in the magnetic field of 1.5 T. The inset shows schematically two paths of radiative transitions of photoelectrons in the Mn doped QW.

polarization of both PL peaks at different temperatures. At low temperature, the polarization of Peak I linearly increases with the magnetic field at small fields and saturates at high fields. With the temperature increase, the polarization decreases and the saturation vanishes. Behavior of Peak II is similar though the polarization at low temperatures can not be reliably determined due to the disappearance of Peak II in the magnetic fields stronger than 1 T.

Sample B with far low Mn doping also demonstrates two PL lines, Fig. 6(a). Peak II is poorly pronounced so that it cannot be analyzed. Peak I demonstrates a blue shift and a strong polarization in the magnetic field ($P_{circ} = 40\%$ at $B = 6$ T). The sign of the polarization is the same as for sample A, but, in contrast to what was observed in sample A, Peak I in sample B exhibits no splitting (Fig. 6(b)) within our spectral resolution of ≈ 0.3 meV.

In reference sample R, PL contour consists of a single narrow peak (Peak I) while Peak II is absent, Fig. 7(a). Application of a magnetic field results in a blue shift of the PL line and a strong circular polarization which reaches 54% in a magnetic field of 6 T. Similar to sample B, no energy splitting of the peak has been detected (Fig. 7(b)).

The large energy splitting and polarization of the PL peaks measured in sample A as well as their field and temperature dependencies point to the important role of the exchange interaction between carriers confined in the

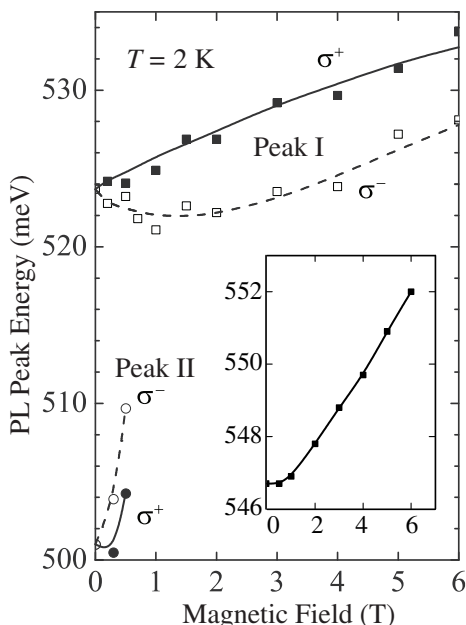


FIG. 3: Energy positions of σ^+ and σ^- components of Peaks I and II as a function of the magnetic field measured in sample A at $T = 2$ K for $W_{exc} = 10$ W/cm². The inset displays the corresponding dependence for structure R. Lines are a guide for the eyes.

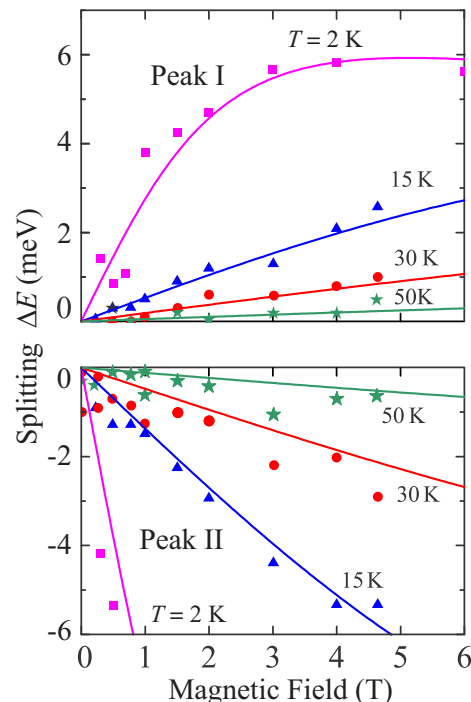


FIG. 4: Magnetic field dependence of the energy splitting ΔE of Peaks I and II, in sample A at different temperatures. ΔE is defined as $E_+ - E_-$, where $E_{+/-}$ is the energy corresponding to the $\sigma^{+/-}$ polarized components. Dots represent the experimental data obtained at different temperatures. Lines correspond to the theoretical fit after Eqs. (6) and (8). The effective temperature T_{Mn} is assumed to be equal to sample temperature T , except at $T = 2$ K, where the best fit corresponds to $T_{Mn} = 3.3$ K.

QW and Mn ions. An independent evidence for substantial exchange interaction has been obtained by studying of magneto-gyrotropic effect [15] in the same structures [9].

V. DISCUSSION

We ascribe Peak I which dominates the PL signal of samples A, B as well as the single PL peak observed from reference structure R to radiative recombination of electrons and heavy holes occupying the ground levels e1 and hh1 in the QW. It should be noted that excitonic effects are negligible in our experiments. Indeed, the exciton binding energy is known to be of the order of 1 meV in InAs QWs whereas the Fermi energy due to the large hole concentration in studied Mn-doped samples is much larger. The density of photoelectrons contributing to radiative recombination is far lower and they seem to be localized with binding energies of a few meV. Localization centers can emerge due to inhomogeneity of the InAs QW and presence of charged ions. This conclusion is confirmed by the quadratic magnetic field dependence of

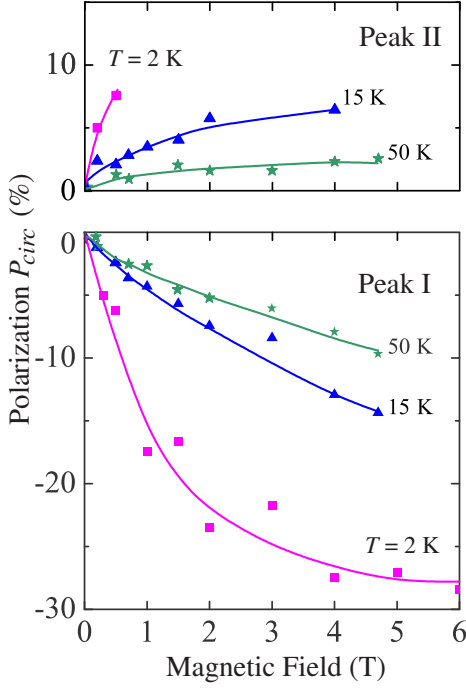


FIG. 5: Polarization degree P_{circ} of both Peaks I and II measured in sample A at $T = 2$ K for $W_{exc} = 10$ W/cm². Lines are a guide for the eyes.

the PL peak energy, observed in a magnetic fields up to $2 \div 3$ T for all studied structures, see Fig. 3 for sample A and the inset of Fig. 3 for sample R. In the case of sample A, the picture is complicated by the superimposed non-linear on B splitting, Fig. 3.

We attribute the red-shifted Peak II, detected in DMS structures, to optical transitions of conduction electrons to the acceptor level of Mn ions, embedded in the QW, see inset of Fig. 2(a). Indeed, a shallow manganese impurity band lying 23 meV below the InAs valence band edge was revealed in bulk InMnAs [16]. Using this value as a reference for the Mn shallow acceptor binding energy in bulk InAs, we have calculated the binding energy E_{Mn} in the QW. For that we followed the method suggested in Ref. [17] and treated the acceptor in zero-range potential approximation. Within the approach the bound state wavefunction Ψ satisfies the Schrödinger equation:

$$H_L \Psi = E_{Mn} \Psi + 2\pi\delta(\mathbf{r} - \mathbf{r}_0) \Psi_0, \quad (1)$$

where H_L is the Luttinger Hamiltonian, \mathbf{r}_0 is the acceptor position. The 4-component function Ψ_0 is to be found from the boundary conditions. At the impurity site \mathbf{r}_0 the boundary condition for the angular averaged wavefunction $\bar{\Psi}$ reads:

$$\bar{\Psi}|_{\mathbf{r} \rightarrow \mathbf{r}_0} = \left(\frac{1}{|\mathbf{r} - \mathbf{r}_0|} - \alpha \right) \Psi_0 + o(|\mathbf{r} - \mathbf{r}_0|), \quad (2)$$

where α is the parameter of the impurity attractive potential strength in the zero-range potential model. At

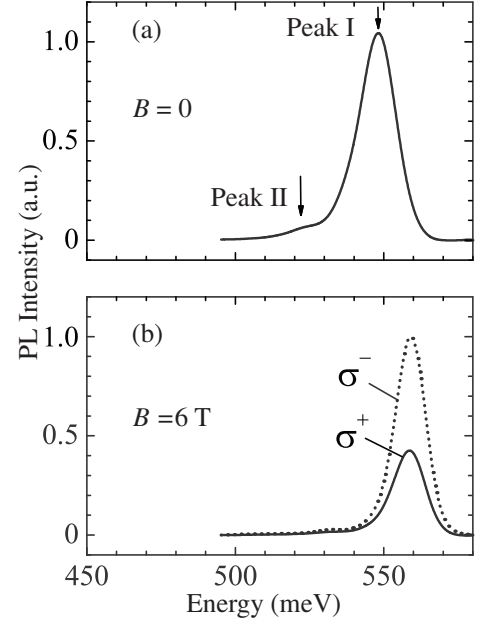


FIG. 6: PL spectra of sample B measured at $T = 2$ K for $W_{exc} = 10$ W/cm². (a) without magnetic field, (b) circularly polarized magneto-PL spectra obtained in a magnetic field of 6 T.

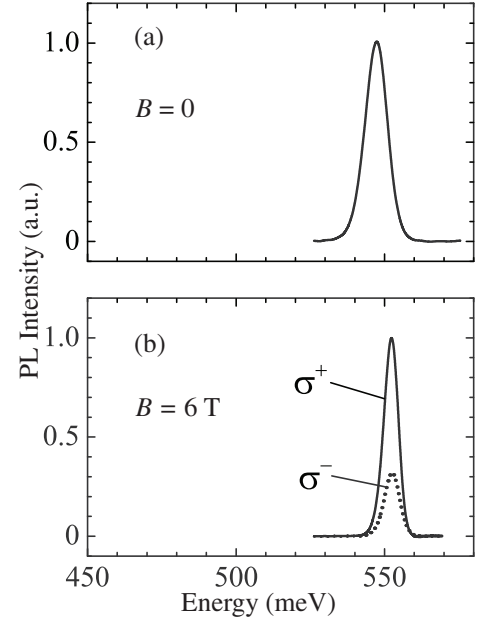


FIG. 7: PL spectra of sample R measured at $T = 2$ K for $W_{exc} = 10$ W/cm². (a) without magnetic field, (b) circularly polarized magneto-PL spectra for $B = 6$ T.

the QW boundaries all components of Ψ were set to zero thus implying the boundary conditions for the infinitely deep QW. Setting the QW width to infinity enabled us to find α from (1),(2) with E_{Mn} being set to the Mn binding energy for the bulk. Restoring the QW width to its experimental value we obtained the binding energy

E_{Mn} from Eq. (1) and (2) with known α . The calculation shows that for the system studied, containing the 4 nm wide QW, E_{Mn} is practically the same as that in bulk InAs, though in narrower QWs it decreases swiftly. The particular value $E_{Mn} \simeq 25$ meV obtained for Mn ion in the center of the 4 nm QW is in good agreement with the experimentally observed red shift of Peak II relative to Peak I. Attribution of Peak II to the presence of Mn in QW is consistent with the fact that Peak II is extremely weak in sample B having lower Mn content.

We now turn to the case of an applied magnetic field. The magneto-PL of the manganese-free structure R was studied in detail in Ref. [11]. Here we give only a brief summary of the main results which are important for the further discussion. The application of a magnetic field results in the spin splitting of both, conduction and valence bands. Optical recombination processes of the electron $|e1, +1/2\rangle$ with the hole $|hh1, -3/2\rangle$ or the electron $|e1, -1/2\rangle$ and the hole $|hh1, +3/2\rangle$ are accompanied by the emission of σ^- - and σ^+ -polarized photons, respectively, that are detected in the Faraday geometry of the experiment. The strong σ^+ circular polarization of the magneto-PL peak stems from the spin polarization of the nonequilibrium holes, characterized by a faster relaxation to the ground Zeeman level in comparison with electrons. The same polarization is observed in structures with degenerate 2DEG, where the different electron spin states are equally populated [11]. The absence of the splitting of the PL line into polarized components of different helicity was explained by the nearly equal magnitude of the electron and hole Lande factors in the system [11]. Within the suggested model, the polarization must invert its sign to σ^- if we change type of conductivity of the QW from n -type to strong p -type. Indeed, at the condition of equally populated spin levels in the valence band in p -type samples, polarization is determined by electrons and recombination of electron at the ground state $|e1, +1/2\rangle$ (for negative electron g -factor) with the hole $|hh1, -3/2\rangle$ must dominate. This process is accompanied by the emission of σ^- -polarized photons. Samples A and B contain degenerated 2DHG, thus σ^- polarization of Peak I detected from these samples is consistent with the model. Zero splitting of circular polarized PL components in sample B should be obviously attributed to vanishingly small Mn content in the InAs QW.

In contrast to sample B, sample A provides clear evidence that free carriers interact via exchange with Mn ions embedded in the InAs QW. Indeed, application of a magnetic field results in a large splitting of Peak I into circularly polarized components (Fig. 4) which is accurately described by the Brillouin function in a wide temperature range (fitting details are given in the next Section). The splitting tends to saturate in magnetic fields higher than $3 \div 4$ T at the lowest achieved temperature of 2 K and decreases rapidly if temperature is raised above ~ 10 K. The polarization dependence on magnetic field and tem-

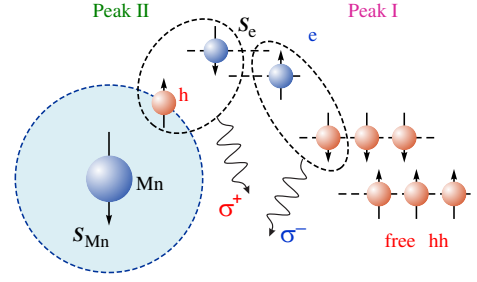


FIG. 8: Sketch of the optical transitions contributing to Peaks I and II in magnetic field. Only transitions contributing to dominant circularly polarized components of Peaks I and II are depicted.

perature is similar to that of the splitting, Fig. 5.

To clarify the role of carrier heating by photoexcitation we have measured the dependence of the polarization degree on magnetic fields up to 6 T at different excitation power in the range $5 \div 10$ W/cm² for sample A and $2.5 \div 10$ W/cm² for sample B. In the first case no difference has been observed for different light intensities. For sample B the peak value of P_{circ} at the lowest excitation level was 10% higher than that for the maximum excitation power while the shape of the curves did not change. Thus the contribution of light heating can be considered as minor.

We note that all the investigated structures show a polarization degree which is considerably below 100% even at $T = 2$ K and $B = 6$ T although the dependence P_{circ} vs B tends to saturate. This fact can be ascribed to the interplay between the short lifetime of photogenerated carriers compared to the spin relaxation time. In the particular case of p -type QWs, where the holes are unpolarized and the PL polarization is determined solely by the electron spin polarization, the PL polarization is given by $P_c = -2S_e^{(0)}\tau_r/(\tau_r + \tau_s)$. Here $S_e^{(0)}$ is the average electron spin in thermal equilibrium, and τ_r and τ_s are the electron lifetime and spin relaxation time, respectively.

Microscopic theory

Now we discuss the microscopic model describing polarization and splitting of Peaks I and II in a magnetic field. Peak II is attributed to the optical transitions between photoelectrons and holes bound to Mn ions (see Fig. 8) which can be schematically described as



where the symbols e , h , and γ denote an electron, hole, and photon, respectively. Mn ion and the hole bound to Mn are antiferromagnetically coupled. In the magnetic field, the bound-hole-Mn complex gets polarized in such a way that the hole spin points along the field

k	Initial state $J_z, s_{e,z}$	Final state $S_{Mn,z}$	Relative rate C_k	Zeeman shift Δ_k
1	-1, -1/2	-5/2	1/2	$-\Delta_e/2 - \Delta_1 + 5\Delta_{Mn}/2$
2	-1, +1/2	-3/2	1/10	$\Delta_e/2 - \Delta_1 + 3\Delta_{Mn}/2$
3	0, -1/2	-3/2	1/5	$-\Delta_e/2 + 3\Delta_{Mn}/2$
4	0, +1/2	-1/2	1/10	$\Delta_e/2 + \Delta_{Mn}/2$
5	+1, -1/2	-1/2	1/20	$-\Delta_e/2 + \Delta_1 + \Delta_{Mn}/2$
6	+1, +1/2	+1/2	1/20	$\Delta_e/2 + \Delta_1 - \Delta_{Mn}/2$

TABLE I: Optical transitions between conduction-band electrons and holes bound to Mn with emission of σ^+ -polarized photons. Δ_e , Δ_1 , and Δ_{Mn} are the Zeeman splitting of electron states, hole-Mn complex, and Mn ion, respectively.

direction. Recombination of spin polarized holes with electrons leads to σ^+ circular polarization of Peak II.

Due to the strong p - d exchange coupling, the ground state of the bound-hole-Mn complex is described by the total angular momentum $J = 1$ and is three-fold degenerate in the projection J_z at zero magnetic field [18]. A conduction-band electron, in contrast, has spin $s_e = 1/2$, and each state is two-fold degenerate. Thus, there are six different initial states for the processes described by Eq. (3). The final electron state of Mn is six-fold degenerate in the projections of the Mn spin $S_{Mn} = 5/2$. The allowed optical transitions emitting σ^+ -polarized radiation (labeled by the index $k = 1 \dots 6$) and their relative intensities C_k are summarized in Table I. The transitions allowing the emission of σ^- -polarized photons can be obtained from Table I by simultaneous inverting the sign of J_z , $s_{e,z}$ and $S_{Mn,z}$.

In an external magnetic field, the emission line splits into 12 components, each of them being either σ^+ - or σ^- -polarized. The corresponding Zeeman shifts of the σ^+ -polarized components are listed in Table I. In a real QW structure, however, individual components may not be spectrally resolved due to considerable inhomogeneous broadening. Therefore, the measured spectrum of the σ^+ -polarized PL is given by

$$I_+(\hbar\omega) = \sum_{k=1}^6 C_k f_k D(\hbar\omega - \Delta_k), \quad (4)$$

where f_k is the population of the initial state with the index k and $D(\hbar\omega)$ is the PL contour at zero magnetic field. To first order in the Zeeman splitting, Eq. (4) is equivalent to

$$I_+(\hbar\omega) \approx D(\hbar\omega) \sum_k C_k f_k - D'(\hbar\omega) \sum_k C_k \Delta_k f_0, \quad (5)$$

where $D'(\hbar\omega) = dD(\hbar\omega)/d\hbar\omega$ and f_0 is the population at zero magnetic field, identical for all initial states. Equation (5) describes that the PL contour $I_+(\hbar\omega)$ is spectrally shifted with respect to the PL contour at zero field by $\sum_k C_k \Delta_k / \sum_k C_k$. Similarly, the σ^- -polarized

PL contour is shifted in the opposite direction by the same value. For the particular case of the optical transitions listed in Table I, the effective Zeeman shift between the broadened PL lines of opposite helicity is given by

$$\Delta E_{II} = -\Delta_1 - \frac{1}{2}\Delta_e + \frac{5}{2}\Delta_{Mn}. \quad (6)$$

The Zeeman splitting of the hole-Mn complex, Mn ion, and conduction-band electron have the form

$$\Delta_1 = g_1 \mu_0 B_z, \quad \Delta_{Mn} = g_0 \mu_0 B_z, \quad (7)$$

$$\Delta_e = g_e \mu_0 B_z + a B_1 \left(\frac{g_1 \mu_0 B_z}{k_B T_{Mn}} \right),$$

where g_1 is the g -factor of the hole-Mn complex, $g_0 = 2$ is the Mn g -factor, g_e is the intrinsic electron g -factor, μ_0 is the Bohr magneton, T_{Mn} is the effective temperature of the Mn spins, and $B_1(x) = 2 \sinh x / (1 + 2 \cosh x)$ is the Brillouin function of the momentum $J = 1$. The second contribution to Δ_e describes the splitting due to exchange interaction between conduction-band electrons and hole-Mn complexes, parameter a depends on the exchange interaction strength and complex concentration.

The PL Peak I is attributed to the optical transitions between electrons and heavy holes confined in the QW, see Fig. 8. The sign of the PL circular polarization in a magnetic field is largely determined by the spin polarization of electrons since the thermal spin polarization of holes is low in p -doped structures. The electron spin polarization can occur due to thermal population of spin-split states as well as spin-dependent extraction of electrons caused by other recombination channels [19], e.g., radiative transitions contributing to Peak II. The spectral shift between the polarized lines of opposite helicity in a magnetic field is determined by the Zeeman splitting of both, conduction and valence bands, and is given by

$$\Delta E_I = -\Delta_e + \Delta_{hh}, \quad (8)$$

where Δ_{hh} is the Zeeman splitting of the heavy-hole subband,

$$\Delta_{hh} = g_{hh} \mu_0 B_z + b B_1 \left(\frac{g_1 \mu_0 B_z}{k_B T_{Mn}} \right), \quad (9)$$

Here, b is the parameter describing the strength of the exchange interaction between free holes and hole-Mn complexes.

Peak I and its splitting in magnetic fields is well observed in experiment. In the regime of small magnetic fields, ΔE_{II} depends linearly on the magnetic field and has two contributions: one is temperature independent and the other one scales as $1/T_{Mn}$. Fitting the experimental data presented in Fig. 4 by Eq. (8) yields $(b - a)g_1 \approx 24$ meV and $g_e - g_{hh} \approx 2.6$. The small

absolute value of $g_e - g_{hh}$ is in agreement with negligible splitting of the PL line in QW structures without magnetic impurities [11]. We note that at temperatures $T < 5$ K, PL spectra are weakly sensitive to the sample temperature. This indicates that the effective Mn temperature T_{Mn} is higher than the nominal sample temperature due to heating by radiation. In particular, the best agreement between the experimental curve measured at 2 K and theory is obtained for an effective temperature $T_{Mn} \approx 3.3$ K. Peak II is less pronounced and disappears in high magnetic fields, therefore its treatment is less reliable. Fitting the data on the Zeeman splitting of Peak II by Eq. (6) yields $ag_1 \approx -126$ meV and $2g_1 + g_e \approx -4.6$.

The saturation of the splitting at higher magnetic fields is determined by g_1 . The best fit of the experimental data for Peak I using $T_{Mn} = 3.3$ K is obtained for $g_1 \approx 3.5$. This value is in agreement with the theoretical calculation for the g -factor of a bound-hole-Mn complex [17]. Taking this g_1 value, all other parameters can be estimated as $a \approx -36$ meV, $b \approx -29$ meV, $g_e \approx -11.6$, and $g_{hh} \approx -14.2$ for the QW structure under study. The negative sign of b is in agreement with the antiferromagnetic behavior of the p - d exchange interaction. The determined negative sign of the parameter a , which describes the exchange interaction between the conduction-band electron and bound-hole-Mn complex, may be caused by the electron-hole exchange interaction and is discussed in Ref. 20.

Surprisingly, the observed splitting of the PL lines in sample A is two orders of magnitude larger than estimated if one uses the $s-d$ and $p-d$ exchange-coupling constants for bulk InMnAs, α and β of order of -1 eV and 0.5 eV, respectively, [6]. One possible explanation for this amazing fact is the inhomogeneous Mn distribution in the plane of the QW. Indeed, even in the case of high quality metamorphic buffer layers used in our structures the density of extended defects (threading dislocations) lies around 10^6 cm $^{-2}$, maximum 10^7 cm $^{-2}$. Due to well-known phenomenon — enhanced metal diffusion and accumulation along the threading dislocations in III-V semiconductors [21, 22] — Mn atoms can accumulate around the residual threading dislocations propagating into the QW. Thus, their local concentration in the InAs Qw can exceed the average level of segregated Mn concentration $\sim 10^{18}$ cm $^{-3}$ and may in principle be high enough to create the regions of InMnAs with Mn content on the order of 1 %.

VI. SUMMARY

To summarize, we have demonstrated that strained InAs QWs with low concentration of manganese ($\sim 0.01\%$) exhibit bright low-temperature photoluminescence. It is shown that the Zeeman effect in such strongly diluted magnetic heterostructures can be accurately in-

vestigated by using magneto-PL as a highly informative method. An anomalously giant splitting of the PL lines in magnetic fields was observed in one of the diluted magnetic InAs QW structures. This surprising finding is ascribed to local Mn accumulation along threading dislocations.

Financial support by the DFG (SFB 689), Russian Foundation for Basic Research, RF President grant MD-3098.2014.2, and EU project SPANGL4Q is gratefully acknowledged.

-
- [1] T. Dietl, *Nature Mat.* **9**, 965 (2010).
 - [2] T. Schallenberg and H. Munekata, *Appl. Phys. Lett.* **89**, 042507 (2006).
 - [3] H. Ohno, H. Munekata, T. Penney, S. von Molnár, and L. L. Chang, *Phys. Rev. Lett.* **68**, 2664 (1992).
 - [4] U. Wurstbauer, C. Śliwa, D. Weiss, T. Dietl, and W. Wegscheider, *Nature Phys.* **6**, 955 (2010).
 - [5] B. Rupperecht, W. Krenner, U. Wurstbauer, Ch. Heyn, T. Windisch, M. A. Wilde, W. Wegscheider and D. Grundler, *J. Appl. Phys.* **107**, 093711 (2010).
 - [6] A. Zudov, J. Kono, Y. H. Matsuda, T. Ikaida, N. Miura, H. Munekata, G. D. Sanders, Y. Sun, and C. J. Stanton, *Phys. Rev. B* **66**, 161307 (2002).
 - [7] V.V. Bel'kov, and S.D. Ganichev, Magneto-gyrotropic effects in semiconductor quantum wells, review. *Semicond. Sci. Technol.* **23**, 114003 (2008).
 - [8] Ya. V. Terent'ev, C. Zoth, V. V. Bel'kov, P. Olbrich, C. Drexler, V. Lechner, P. Lutz, M. S. Mukhin, S. A. Tarasenko, A. N. Semenov, V. A. Solov'ev, I. V. Sedova, G. V. Klimko, T. A. Komissarova, S. V. Ivanov, and S. D. Ganichev, *Appl. Phys. Lett.* **99**, 072111 (2011).
 - [9] P. Olbrich, C. Zoth, P. Lutz, C. Drexler, V. V. Bel'kov, Ya. V. Terent'ev, S. A. Tarasenko, A. N. Semenov, S. V. Ivanov, D. R. Yakovlev, T. Wojtowicz, U. Wurstbauer, D. Schuh, and S. D. Ganichev, *Phys. Rev. B* **86**, 085310 (2012).
 - [10] G. A. Khodaparast, Y. H. Matsuda, D. Saha, G. D. Sanders, C. J. Stanton, H. Saito, S. Takeyama, T. R. Merritt, C. Feeser, B. W. Wessels, X. Liu, and J. Furdyna, *Phys. Rev. B* **88**, 235204 (2013).
 - [11] Ya. V. Terent'ev, S. N. Danilov, J. Lohr, D. Schuh, D. Bougeard, D. Weiss, M. V. Durnev, S. A. Tarasenko, M. S. Mukhin, S. V. Ivanov, and S. D. Ganichev, *Appl. Phys. Lett.* **104**, 101111 (2014).
 - [12] U. Wurstbauer, M. Soda, R. Jakiela, D. Schuh, D. Weiss, J. Zweck, and W. Wegscheider, *J. of Cryst. Growth* **311**, 2160 (2009).
 - [13] J. Karch, C. Drexler, P. Olbrich, M. Fehrenbacher, M. Hirmer, M. M. Glazov, S. A. Tarasenko, E. L. Ivchenko, B. Birkner, J. Eroms, D. Weiss, R. Yakimova, S. Lara-Avila, S. Kubatkin, M. Ostler, T. Seyller, S. D. Ganichev, *Phys. Rev. Lett.* **107**, 276601 (2011).
 - [14] M.M. Glazov and S.D. Ganichev, *Physics Reports* **535**, 101 (2014).
 - [15] S.D. Ganichev, S.A. Tarasenko, V.V. Bel'kov, P. Olbrich, W. Eder, D.R. Yakovlev, V. Kolkovsky, W. Zaleszczyk, G. Karczewski, T. Wojtowicz, and D. Weiss, Spin currents in diluted magnetic semiconductors. *Phys. Rev.*

- Lett. **102**, 156602 (2009).
- [16] P. T. Chiu, A. J. Blattner, S. J. May, and B. W. Wessels, *Physica B* **344**, 379 (2004).
 - [17] N. S. Averkiev, A. E. Zhukov, Yu. L. Ivanov, P. V. Petrov, K. S. Romanov, A. A. Tonkikh, V. M. Ustinov, G. E. Tsyrlin, *Semiconductors* **38**, 217 (2004).
 - [18] N. S. Averkiev, A. A. Gutkin, E. B. Osipov, M. A. Reshchikov, *Sov. Phys. Solid State* **30**, 438 (1988).
 - [19] V. L. Korenev, I. A. Akimov, S. V. Zaitsev, V. F. Sapega, L. Langer, D. R. Yakovlev, Yu. A. Danilov, and M. Bayer, *Nature Commun.* **3**, 959 (2012).
 - [20] C. Śliwa and T. Dietl, *Phys. Rev. B* **78**, 165205 (2008).
 - [21] Z. Liliental-Weber, J. Jasinski, J. Washburn, *J. Cryst. Growth* **246**, 259 (2002).
 - [22] S. V. Ivanov, T. V. Shubina, V. N. Jmerik, V. A. Vekshin, P. S. Kop'ev, B. Monemar, *J. of Cryst. Growth* **269**, 1 (2004).